












PAPER

[View Article Online](#)
[View Journal](#) | [View Issue](#)Cite this: *Dalton Trans.*, 2023, **52**,
8332Interesting chemical and physical features of the
products of the reactions between trivalent
lanthanoids and a tetradentate Schiff base derived
from cyclohexane-1,2-diamine†Ioannis Mylonas-Margaritis, ^{a*} Zoi G. Lada, ^b Alexandros A. Kitos, ^a
Diamantoula Maniaki, ^a Katerina Skordi,^c Anastasios J. Tasiopoulos, ^c
Vlasoula Bekiari, ^d Albert Escuer, ^e Julia Mayans, ^{*e}
Vassilios Nastopoulos, ^{a*} Evangelos G. Bakalbassis,^{*f} Dionissios Papaioannou ^{*a}
and Spyros P. Perlepes ^{*a,b}

The initial use of a tetradentate Schiff base (LH₂) derived from the 2 : 1 condensation between 2-hydroxyacetophenone and cyclohexane-1,2-diamine in 4f-metal chemistry is described. The 1 : 2 reaction of Ln(NO₃)₃·xH₂O (Ln = lanthanoid or yttrium) and LH₂ in MeOH/CH₂Cl₂ has provided access to isostructural complexes [Ln(NO₃)₃(L'H₂)(MeOH)] in moderate to good yields. Surprisingly, the products contain the corresponding Schiff base ligand L'H₂ possessing six aliphatic –CH₂– groups instead of the –CH–(CH₂)₄–CH– unit of the cyclohexane ring, i.e. an unusual ring-opening of the latter has occurred. A mechanism for this Ln^{III}-assisted/promoted LH₂ → L'H₂ transformation has been proposed assuming transient Ln^{II} species and a second LH₂ molecule as the H₂ source for the reduction of the cyclohexane moiety. DFT calculations provide strong evidence for the great thermodynamic stability of the products in comparison with analogous complexes containing the original intact ligand. The structures of the Pr^{III}, Sm^{III}, Gd^{III}, Tb^{III}, and Ho^{III} complexes have been determined by single-crystal X-ray crystallography. The 9-coordinate Ln^{III} centre in the molecules is bound to six oxygen atoms from the three bidentate chelating nitrato groups, two oxygen atoms that belong to the bidentate chelating organic ligand, and one oxygen atom from the coordinated MeOH group. In the overall neutral bis(zwitterionic) L'H₂ ligand, the acidic H atoms are clearly located on the imino nitrogen atoms and this results in the formation of an unusual 16-membered chelating ring. The coordination polyhedra defined by the nine donor atoms around the 4f-metal-ion centres can be best described as distorted, spherical capped square antiprisms. The Eu^{III}, Tb^{III}, and Dy^{III} complexes exhibit Ln^{III}-based luminescence in the visible region, with the coordinated L'H₂ molecule acting as the antenna. Ac magnetometry experiments show that the Dy^{III} member of the family behaves as an SIM at zero field and under external dc fields of 0.1 and 0.2 T without the enhancement of the peaks' maxima, suggesting that QTM is not the relaxation path. The Gd^{III} complex behaves, rather unexpectedly, as a SIM with two different magnetic relaxation paths occurring at very close temperatures; this behaviour is tentatively attributed to a very small axial zero-field splitting (*D* ~ 0.1 cm^{–1}), which cannot be detected by magnetization or susceptibility experiments. The prospects of the present, first results in the lanthanoid(III)-LH₂ chemistry are discussed.

Received 17th March 2023,

Accepted 13th May 2023

DOI: 10.1039/d3dt00817g

rsc.li/dalton^aDepartment of Chemistry, University of Patras, 26504 Patras, Greece.E-mail: ioanismoymargaritis@gmail.com, dapapaio@upatras.gr,
nastopoulos@upatras.gr, perlepes@upatras.gr, bakalbas@chem.auth.gr^bInstitute of Chemical Engineering Sciences (ICE-HT), Foundation for Research and
Technology-Hellas (FORTH), P.O. Box 1414, Platani, 26504 Patras, Greece^cDepartment of Chemistry, University of Cyprus, 1678 Nicosia, Cyprus^dDepartment of Agriculture, University of Patras, 26504 Patras, Greece^eDepartment de Química Inorgànica i Organica, Secio Inorgànica and Institute of
Nanoscience (IN2UB) and Nanotechnology, Universitat de Barcelona, Martí i

Franques 1-11, 08028 Barcelona, Spain. E-mail: julia.mayans@qi.ub.edu

^fDepartment of Chemistry, Aristotle University of Thessaloniki, University Campus,

54124 Thessaloniki, Greece. E-mail: bakalbas@chem.auth.gr

†Electronic supplementary information (ESI) available: Crystallographic
(Table S1) and structural data (Tables S2 and S13), various spectra (Fig. S1–S4,
S10–S12), structural plots (Fig. S5–S9 and S16–S19), magnetic plots (Fig. S13–
S15), mechanistic schemes (Schemes S1–S6), and computational drawings
(Schemes S7 and S8). CCDC 2246267–2246271. For ESI and crystallographic data
in CIF or other electronic format see DOI: <https://doi.org/10.1039/d3dt00817g>

Introduction

Inorganic chemistry was dominated by transition metals (3d, 4d, 5d) in the second half of the 20th century.¹ In the last 20 years or so, there has been a considerable shift of focus on the chemistry of f metals, mainly that of lanthanoids (Ln's).² When scientists, including S. P. P. (the co-author of this paper), started working in the Ln metal area in the early 1980s, they were told that this chemistry had no future.³ Today, the opposite is true! The Ln elements exhibit pronounced chemical similarities as a group near the bottom of the periodic table, but simultaneously they express distinctive and varied electronic properties. These atomistic properties are very useful and are the basis for application in many technological areas, including the construction of devices.⁴ The chemical (production of fine chemicals, catalytic activity, reactivity, bonding models), optical (optical fiber Er amplifiers, phosphors, luminescence thermometers, lasers, coloured ceramics, and glasses), quantum (atomic clocks, trapped ¹⁷¹Yb⁺ qubits, time crystals), mechanical (polishing powders, metallurgy, alloys with special characteristics), magnetic (Gd^{III}-MRI agents, high Tc superconductors, hard magnets such as Nd₂Fe₁₄B, single-molecule magnets (SMMs), single-ion magnets), and biological (methanol dehydrogenase, Ln³⁺-dependent bacteria) properties of the metals and their ions are exploited in various areas of technology and fundamental research.^{3,4} The shielded nature of the 4f orbitals results in well-defined energy levels that are weakly perturbed by the coordination environment and are accompanied by large spin-orbit coupling; these characteristics enable the exploitation of Ln³⁺ ions in optical and magnetic applications. The magnetic and luminescence properties of some members of a new family of Ln^{III} complexes are part of the present work.

As far as the magnetic properties of molecular Ln^{III} complexes are concerned, the discovery of slow relaxation of the magnetization and magnetic hysteresis in a bis(phthalocyaninato)terbium(III) complex in 2003⁵ ignited an explosive growth of research interest in Ln^{III}-based molecular nanomagnets, either coordination clusters (single-molecule magnets, SMMs) or mononuclear complexes (single-ion magnets, SIMs), because of their exciting physical phenomena and potential applications in magnetic memory storage, molecular spintronics, and quantum computing.^{6,7} Design principles developed by Rinehart and Long directed synthetic chemists and physicists towards longer relaxation times by means of extremely large increases in the energy barrier to magnetization reversal (U_{eff}).⁸ The massive increases did not lead to corresponding increases in the blocking temperature (T_{B}) due to the vibronically-induced spin relaxation mechanisms – irrespective of the U_{eff} value – that can operate.⁹ A breakthrough happened in 2017 when it was shown¹⁰ that the cation $[\text{Dy}(\text{C}_{\text{p}}^{\text{ttt}})_2]^+$, where $\text{C}_{\text{p}}^{\text{ttt}}$ is $\text{C}_5\text{H}_5^t\text{Bu-1,2,4}$, exhibits magnetic hysteresis up to 60 K. Subsequent studies showed impressive results in this area.^{11a,b} Removal of C–H groups from the C_5 ring of $\text{C}_{\text{p}}^{\text{ttt}}$ through the synthesis of peralkylated bis(cyclopentadienyl) Dy^{III} complexes led to hysteresis temperatures T_{B} around the ligand nitrogen temperature (~ 80 K), which is the current record.^{11c}

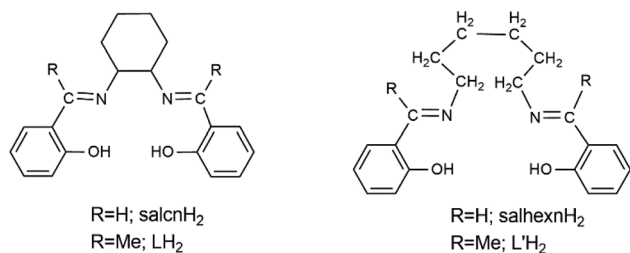
As far as the optical properties are concerned, most Ln^{III} ions luminesce in the solid state. Unlike luminescence from organic compounds, most 4f-metal ion emissions consist of sharp lines. This property has been used in Eu^{III} and Tb^{III} phosphors, and in the Nd^{III} YAG laser. Eu^{III} and Tb^{III}, and sometimes Dy^{III}, display luminescence in the visible region.¹² The 4f → 4f transitions are Laporte forbidden and thus excitation of Ln^{III} to an emissive state by this route is not an efficient process. An alternative method of excitation is *via* an organic ligand, usually an aromatic system, which has an excited triplet state higher in energy than the Ln^{III} emissive state, the so-called antenna effect.¹³

We are interested in mononuclear Ln^{III} complexes that show magnetic relaxation (SIMs) and/or Ln^{III}-based luminescence. For the realization of this general goal, the choice of the primary organic ligand is very important. For the preparation of SIMs, the ligand should behave as terminal (either monodentate or chelating). It is also crucial for the appearance of the required magnetic anisotropy of the molecule and a high separation between M_j and $M_j \pm 1$ states (in order to obtain high U_{eff} values), and these imply a rational design of the ligand field. For oblate-type ions (*e.g.* Tb^{III} and Dy^{III}), the ligand donor atoms with the greatest electron density should bind at axial positions enhancing the required axial anisotropy, whereas for prolate-type ions (*e.g.* Er^{III} and Yb^{III}), the ligand donor atoms with the largest electron density should coordinate to equatorial positions to achieve axial anisotropy. For the synthesis of luminescent Ln^{III} complexes with metal ion-based emission, the ligands should bear chromophores which can facilitate efficient energy transfer “sensitization” of the Ln^{III} ion's excited (*i.e.* emissive) levels from the ligand's triplet state. Schiff bases are often used for these purposes.¹⁴ We have been using Schiff bases of various types to achieve the above-mentioned objectives.¹⁵

We would also like to mention that the chemistry of mononuclear Ln^{III}-Schiff base complexes is attracting the interest of inorganic chemists for two additional reasons. First, it has been shown that two and four electrons can be stored, respectively, in intramolecular and intermolecular C–C bonds formed by Ln^{III}-assisted reduction of the imino group of Schiff-base ligands, providing new synthetic avenues to the reductive chemistry of lanthanoids.¹⁶ Second, complexes of Yb^{III} with chelating Schiff bases are qubit candidates because of the huge splitting between the electronic ground doublet and the first excited crystal field state and their intrinsic slow paramagnetic relaxation,¹⁷ as well as candidates for novel coupled electronic qubit-nuclear qubit systems.¹⁸

We have recently embarked on a new subarea of Ln^{III}-Schiff base chemistry by using *N,N'*-bis(salicylidene)ethylenediamine (salen)-type ligands, in which non-conjugated, *e.g.* cyclohexyl, bridges are linked with two salicylaldehyde moieties functionalised either on the aromatic rings and/or at the aliphatic carbon atoms. Our general goal is to compare the magnetic (*e.g.* SIM responses) and optical (*e.g.* aggregation-induced emission, AIE, or aggregation-caused quenching, ACQ, behaviour¹⁹) properties of the Ln^{III} complexes containing functiona-





Scheme 1 General structural formulae and abbreviations of the Schiff bases discussed in this work. In the complexes reported in this work, L' H₂ exists in the overall neutral, bis(zwitterionic) form (*vide infra*).

lized Schiff bases with those of the corresponding complexes containing non-functionalized ligands. We plan to use various electron-accepting (–NO₂, –F, –Cl, –CN, –Ph), electron-donating (–OMe, –OH, –NEt₂, –Me) or bulky (*e.g.* ^tBu) substituents. This work started with the reactions of lanthanoid(III) nitrates with the Schiff base LH₂ (Scheme 1), which possesses methyl groups at the aliphatic carbon atoms of the salicylaldehyde moiety. No Ln^{III} complexes of the neutral or anionic forms of LH₂ have been reported; in contrast, Ln^{III} complexes of salcnH₂ or salcn^{2–}, *i.e.* the unsubstituted Schiff base, have been synthesized and structurally characterised, and their emission and magnetic properties were studied.²⁰ However, we were surprised to discover that LH₂ undergoes a Ln^{III}-promoted/assisted cyclohexane ring opening and the isolated complexes contain a neutral L'H₂ ligand (Scheme 1). The interesting structural features and properties (optical, magnetic) of the products are described in this article.

Experimental section

Chemicals and instrumentation

All manipulations were performed under aerobic conditions using materials and solvents (reagent grade) as received. The free organic ligand (*E,E*)-2,2'-(1,1'-(cyclohexane-1,2-diyl)dinitrilo)diethylidinediphenol (LH₂, Scheme 1)²¹ was synthesized by the 2 : 1 condensation reaction between 2-hydroxyacetophenone and (±)-*trans*-1,2-diaminocyclohexane in refluxing MeOH for 8 h; typical yields were in the 65–75% range. Its purity was checked by elemental analysis (C, H, N), and IR and ¹H NMR (*d*₆-DMSO) spectroscopy. Elemental microanalyses (C, H, N) were performed at the Instrumental Analysis Laboratory of the University of Patras. Conductivity measurements were performed at 25 ± 1 °C with a Metrohm-Herisau E-527 bridge and a cell of standard constant using DMSO as the solvent. FT-IR spectra (4000–400 cm^{–1}) were recorded using a PerkinElmer spectrometer with the samples being in the form of KBr pellets. FT-Raman spectra were recorded using an EQUINOX spectrometer to which a Bruker (D) FRA-106/S component was attached. A R510 diode-pumped Nd:YAG laser was used for Raman excitation at 1064 nm with a maximum power of 500 mW on the samples, utilizing an average of 100 scans at 4 cm^{–1} resolution. ¹H NMR and ¹³C NMR spectra were

recorded at 600 and 150 MHz, respectively, on a Bruker Avance III HD spectrometer; the signal of the undeuterated portion of *d*₆-DMSO at δ 2.52 ppm was used as the ¹H NMR reference. Excitation and emission spectra were recorded using a Cary Eclipse fluorescence spectrometer. Solid-state, variable-temperature and variable-field direct current (dc) magnetic data were collected on the powdered samples using a MPMS5 Quantum Design magnetometer operating at 0.03 T in the 300–2.0 K range for the magnetic susceptibility measurements and at 2.0 K in the 0–5 T range for the magnetization experiments. Diamagnetic corrections were applied to the observed susceptibilities using Pascal's constants. Alternating current (ac) magnetic susceptibility experiments were carried out in the 10–1488 Hz frequency range.

Synthetic procedures

Preparation of the representative complex [Pr(NO₃)₃(L'H₂)(MeOH)] (1). To a stirred yellow solution of LH₂ (0.070 g, 0.20 mmol) in a solvent mixture comprising CH₂Cl₂ (30 mL) and MeOH (5 mL) was added solid Pr(NO₃)₃·6H₂O (0.044 g, 0.10 mmol). The solid soon dissolved and the resulting yellow solution was stirred for a further 15 min, filtered and stored in a closed flask. X-ray quality yellow crystals were obtained in a period of 20 d. The crystals were collected by filtration, washed with cold CH₂Cl₂ (1 mL) and Et₂O (3 × 2 mL), and dried in air overnight. The yield was ~55% (based on Pr^{III} available). Analytical data, calcd for C₂₃H₃₂PrN₅O₁₂ (found values are in parentheses): C 38.82 (39.07), H 4.54 (4.48), N 9.85 (9.61)%. Λ_M (DMSO, 10^{–3} M, 25 °C) = 101 S cm² mol^{–1}. IR bands (KBr, cm^{–1}): 3446wb, 3185wb, 3075wb, 2936m, 2862w, 1608s, 1542s, 1462sb, 1342sh, 1300s, 1262sh, 1212m, 1156m, 1066m, 1028s, 952m, 848m, 816m, 756s, 734sh, 620w, 580m, 560m, 528w, 426m, 407sh. Raman peaks (cm^{–1}): 3067m, 2953m, 2924m, 1611s, 1541m, 1503sh, 1447m, 1420sh, 1320s, 1267w, 1244m, 1198m, 1088s, 963w, 843w, 735w, 712s, 562m, 526w, 436m, 404sh, 307w, 249m, 127m.

Preparation of the complexes [Ln(NO₃)₃(L'H₂)(MeOH)] (Ln = Nd, 2; Ln = Sm, 3; Ln = Eu, 4; Ln = Gd, 5; Ln = Tb, 6; Ln = Dy, 7; Ln = Ho, 8; Ln = Er, 9; Ln = Yb, 10; Ln = Y, 11). These complexes were prepared and isolated in an identical manner with **1** by simply replacing Pr(NO₃)₃·6H₂O with the corresponding hydrated nitrate salts (hexa- or pentahydrated) of the other Ln^{III} and Y^{III} ions. Typical yields of the yellow products are in the 40–65% range. The Λ_M (DMSO, 10^{–3} M, 25 °C) values are in the range of 85–110 S cm² mol^{–1}. The IR spectra of **2–11** are almost superimposable with the spectrum of **1** in the 3000–400 cm^{–1} region with a maximum wavenumber difference of ±5 cm^{–1}. The wavenumbers of the Raman peaks of **3**, **7** and **10** are almost identical to those in the spectrum of **1**, albeit with some differences in the relative intensities.

Analytical data, calcd for C₂₃H₃₂LnN₅O₁₂ (found values are in parentheses): **2**: C 38.64 (39.13), H 4.52 (4.47), N 9.80 (9.66); **3**: C 38.31 (37.99), H 4.48 (4.59), N 9.72 (9.63); **4**: C 38.24 (38.57), H 4.47 (4.56), N 9.69 (9.75); **5**: C 37.95 (37.43), H 4.47 (4.41), N 9.62 (9.39); **6**: C 37.86 (37.98), H 4.43 (4.52), N 9.60 (9.41); **7**: C 37.68 (37.92), H 4.41 (4.32), N 9.56 (9.48); **8**: C 37.56



(38.09), H 4.39 (4.28), N 9.52 (9.40); **9**: C 37.44 (37.80), H 4.38 (4.49), N 9.49 (9.52); **10**: C 37.15 (36.99), H 4.35 (4.38), N 9.42 (9.29); **11**: C 41.88 (42.04), H 4.90 (4.81), N 10.62 (10.55)%.

¹H NMR data (*d*₆-DMSO, δ /ppm) for Y^{III} complex **11**. 13.58 (br.s., 2H), 7.40–7.25 (m, 4H), 6.85–6.67 (m, 4H), ~4.9 (br.s., 1H), 3.53 (td, 4H), 2.47 (s, 6H), 1.61 (dd, 4H), 1.50–1.31 (m, 4H). The signal of the –CH₃ protons of MeOH is masked by the intense signal of H₂O (contained in the solvent) at δ ~3.4 ppm.

Preparation of complex [Y(NO₃)₃(LH₂)(H₂O)] (11a). To a stirred yellow solution of LH₂ (0.105 g, 0.30 mmol) in MeCN (6 mL) was added a solution of Y(NO₃)₃·6H₂O (0.057 g, 0.15 mmol) in the same solvent. A yellow solid was immediately precipitated. The reaction mixture was stirred for a further 10 min and the precipitate was collected by filtration, washed with MeCN (2 × 1 mL) and Et₂O (4 × 2 mL), and dried in air for 24 h. The yield was ~65% (based on the Y^{III} available). Analytical data, calcd for C₂₂H₃₀YN₅O₁₂ (found values are in parentheses): C 40.93 (40.71), H 4.69 (4.76), N 10.85 (10.69)%. IR bands (KBr, cm⁻¹): 3507wb, 3370wb, 2937w, 2863w, 1609s, 1545m, 1492m, 1416w, 1346m, 1297m, 1264w, 1215m, 1157m, 1068w, 1031m, 940w, 860m, 818w, 751m, 735w, 621w, 581m, 536w, 451w, 414w, 401sh. ¹H NMR (*d*₆-DMSO, δ /ppm). 13.60 (br.s., 2H), 7.42–7.24 (m, 4H), 6.89–6.69 (m, 4H), 3.58 (t, 4H), 2.46 (s, 6H), 1.64 (dd, 4H), 1.50–1.30 (m, 4H). The same complex can be prepared and isolated in an identical manner by simply replacing MeCN with a solvent mixture containing Me₂CO (4 mL) and CH₂Cl₂ (4 mL). The IR and ¹H NMR spectra of this sample are identical to the spectra obtained using only MeCN as the solvent. The Λ_M (DMSO, 10⁻³ M, 25 °C) values for both samples are ~100 S cm² mol⁻¹.

Preparation of complex [Y(NO₃)₃(LH₂)(CD₃OD)] (11b). To a stirred yellow solution of LH₂ (0.105 g, 0.30 mmol) in a solvent mixture comprising CH₂Cl₂ (3 mL) and CD₃OD (4 mL) was added solid Y(NO₃)₃·6H₂O (0.057 g, 0.15 mmol). The solid dissolved immediately with a simultaneous precipitation of a yellow solid. The solid was collected by filtration, washed with cold CH₂Cl₂ (1 mL) and dried at 60 °C for 2 h. Analytical data, calcd for C₂₂H₂₆D₄N₅O₁₂Y (found values are in parentheses): C 40.68 (40.81), H 4.04 (3.91), N 10.78 (10.71). The IR spectrum of the sample was very similar to that of **11**, with a notable difference being the appearance of a weak to medium band at 2141 cm⁻¹ assigned to ν (CD) of deuteriated methanol. The ¹H NMR spectrum of **11b** was almost identical to that of **11**, with a difference being the decrease of the broad signal at δ ~4.9 ppm in the former attributable to the methanol –OH proton in the latter.

Single-crystal X-ray crystallography

Single crystals of complexes **1**, **3**, **5**, **6** and **8** were coated with paratone-N oil and attached to cryo-loops at the end of a copper pin. Diffraction data were collected by the ω -scan technique on a SuperNova Rigaku diffractometer under a stream of nitrogen gas at 100(2) K using Mo K α radiation (λ = 0.7107 Å), except for compound **8** where Cu K α radiation (λ = 1.5418 Å) was used. Data were collected and processed by the CRYSLIS

CCD and RED software,²² respectively. An empirical absorption correction using spherical harmonics, implemented in SCALE3 ABSPACK scaling algorithm, was applied to the intensities of the collected reflections. All structures were solved with SHELXT^{23a} and refined by full-matrix least-squares techniques on F^2 with SHELXL.^{23b} All non-H atoms were refined anisotropically. Carbon-bound H atoms were included in the calculated positions (riding model). The H atoms on the protonated imino nitrogen atoms of L/H₂, together with the hydroxyl H atoms of the coordinated MeOH molecule in all five structures, were located in difference Fourier maps and refined isotropically applying soft distance restraints (DFIX). Geometric/crystallographic calculations were carried out using PLATON,²⁴ Olex²⁵ and WINGX²⁶ packages. Molecular/packing graphics were prepared with DIAMOND²⁷ and MERCURY.²⁸

Important crystallographic data are listed in Table S1.† Full details can be found in the CIF files. Crystallographic data for the structures reported in this paper have been deposited with the Cambridge Crystallographic Data Centre as supplementary publication with the deposition numbers 2246267–2246271.†

Computational details

DFT calculations for complex **1**, employing the B3LYP functional with the 6-31+G (for the carbon, oxygen and nitrogen atoms) and 6-31G (for the hydrogen atoms) basis sets, were carried out with Gaussian09 (version B.01).²⁹ Moreover, the effective core potential of the Stuttgart group,³⁰ in which the 4f wave functions are imbedded in the core in an effective way – greatly simplifying the calculations without any loss of accuracy – was used for the Pr^{III} ion. Analytical frequencies were calculated at the same level of theory, and the nature of the stationary points was determined according to the number of negative eigenvalues of the Hessian matrix (*i.e.*, no imaginary frequency for the local minimum and one imaginary frequency for transition states). The relative stability of the two complexes (both the experimental structure and a similar one containing the initially used ligand) was calculated based on the free energy values (Gibbs).

Results and discussion

Brief synthetic procedures

The reactions of Ln(NO₃)₃·*x*H₂O (*x* = 5 or 6) or Y(NO₃)₃·6H₂O and LH₂ in a 1:2 molar ratio in CH₂Cl₂/MeOH gave yellow solutions that upon storage at room temperatures gave yellow crystals or crystalline powders of [Ln(NO₃)₃(LH₂)(MeOH)] (**1–10**) or [Y(NO₃)₃(LH₂)(MeOH)] (**11**) in moderate to good yields (40–65%). The crystals of the Pr^{III}, Sm^{III}, Gd^{III}, Tb^{III} and Ho^{III} compounds (complexes **1**, **3**, **5**, **6** and **8**, respectively) were of X-ray quality and their structures were solved by X-ray crystallography. The other six complexes are proposed to be isostructural with **1**, **3**, **5**, **6** and **8** based on elemental analyses and the identical IR spectra. Three synthetic points are of interest: (i) the experimental reaction ratio used (Ln^{III}: LH₂ = 1:2) is not the same with the stoichiometric ratio (Ln^{III}: L/H₂



= 1 : 1); the use of the stoichiometric molar ratio results in the isolation of the same products albeit with much lower yields. (ii) The molecules of the complexes do not contain the initial ligand LH_2 , but instead the transformed ligand $\text{L}'\text{H}_2$ (Scheme 1; *vide supra*). (iii) Complex $[\text{Y}(\text{NO}_3)_3(\text{L}'\text{H}_2)(\text{H}_2\text{O})]$ (**11a**), *i.e.* the aquo analogue of **11**, can be prepared by the 1 : 2 reaction between $\text{Y}(\text{NO}_3)_3 \cdot 6\text{H}_2\text{O}$ and LH_2 in MeCN or $\text{Me}_2\text{CO}-\text{CH}_2\text{Cl}_2$. This fact has implications in the mechanistic proposal (see the ESI†). Since the slow evaporation (almost until dryness) of the solvents from a $\text{CH}_2\text{Cl}_2/\text{MeOH}$ solution containing only LH_2 results in the precipitation of this ligand (IR and ^1H NMR evidence), *i.e.* the used ligand, we propose that the unique $\text{LH}_2 \rightarrow \text{L}'\text{H}_2$ transformation is Ln^{III} -assisted; our mechanistic proposal (ESI†) is based on this assumption. Synthetic organic chemistry has witnessed an explosive growth from the use of lanthanoid(III) reagents.³¹ This transformation (or a similar transformation involving salenH_2 , Scheme 1) has never been observed in the coordination chemistry of LH_2 . DFT calculations (ESI†) reveal the greater thermodynamic stability of complex **1** compared with that of a structurally similar, hypothetical Pr^{III} complex possessing the initially used LH_2 ligand in its bis(zwitterionic) O,O' -bidentate chelating mode, three bidentate chelating nitrato groups and one MeOH ligand. This difference in stability explains the Ln^{III} -assisted/promoted $\text{LH}_2 \rightarrow \text{L}'\text{H}_2$ transformation.

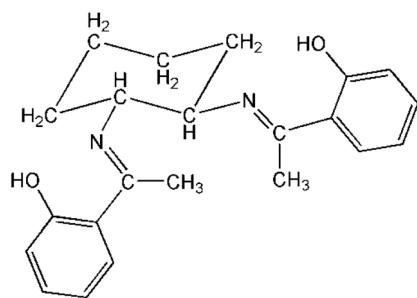
Since the observed transformation was totally unexpected, we re-examined carefully the purity of LH_2 . Also we examined the purity of the 1,2-diaminocyclohexane precursor to investigate if it contained a portion of 1,6-diaminohexane whose condensation with 2-hydroxyacetophenone would have given $\text{L}'\text{H}_2$ as a contaminant of LH_2 ; in the case of contamination, the $\text{L}'\text{H}_2$ component of the mixture with LH_2 would result in the isolation of **1–11**. Our studies proved the purity of LH_2 and its 1,2-diaminocyclohexane precursor. Thus, (1) LH_2 was obtained in the form of yellow single crystals; the unit cell determination of a few of them revealed that they represent²¹ the structurally characterised compound (*E,E*)-2,2'-[1,1'-(cyclohexane-1,2-diyl-dinitrilo)diethylidene]diphenol (Scheme 2); for the preparation of the complex, we used batches of single crystals which were subsequently powdered. (2) The ^1H NMR spectrum of the used powder in d_6 -DMSO shows the expected³² signals for pure LH_2 with the correct integration ratio; there are four signals in the

aromatic region (δ 7.54–6.83 ppm) representing eight protons, a doublet of doublet signal at δ 4.02 ppm due to the two protons attached to positions 1 and 2 of the cyclohexane ring, a singlet signal at δ 2.38 ppm representing the six protons of the two methyl groups and a group of three multiplet signals at δ values of 2.07 (four protons), 1.84 (two protons) and 1.64 (two protons) ppm which represent the eight $-\text{CH}_2-$ protons of the cyclohexane ring. The broad singlet at $\delta \sim 13.5$ ppm (two protons) is assigned¹⁹ to the $-\text{OH}$ hydrogen atoms. (3) The ^1H NMR spectrum of (\pm)-*trans*-1,2-diaminocyclohexane (used for the synthesis of LH_2) in d_6 -DMSO confirms its purity. The spectrum (Fig. S1†) shows five multiplet signals at δ 2.03, 1.70, 1.58, 1.17 and 0.96 ppm with an integration ratio of 1 : 1 : 1 : 1 : 1 (or 2 : 2 : 2 : 2 : 2). The signal at a lower field (δ 2.03 ppm) represents the two protons at the 1 and 2 positions of the cyclohexane ring (*i.e.* the protons belonging to the carbon atoms attached to the two nitrogen atoms), while the other signals correspond to the eight $-\text{CH}_2-$ protons. The $-\text{NH}_2$ protons do not appear because of their exchangeable character. The spectrum is identical (as expected) to the spectra of the pure (+)-*S,S-trans* (Fig. S2†) and (–)-*R,R-trans* enantiomers of 1,2-diaminocyclohexane (provided by Fluorochem). Moreover, this spectrum is different from the recorded spectrum of 1,6-diaminohexane in d_6 -DMSO; the latter shows a triple signal at δ 2.68, a multiplet at δ 1.35 and a multiplet at δ 1.12 with an integration ratio of 1 : 1 : 1 (or 4 : 4 : 4) attributed to the twelve $-(\text{CH}_2)-$ protons. (4) The ^{13}C NMR spectrum of (\pm)-*trans*-1,2-diaminocyclohexane, in d_6 -DMSO (Fig. S3†), which is again identical to the ^{13}C NMR spectra of the pure (+)-*S,S-trans* and (–)-*R,R-trans*, (Fig. S4†) enantiomers, shows the three expected signals of the cyclohexane ring at δ values of 58.1, 35.4 and 25.7 ppm, the former being assigned to the carbons attached to the nitrogen atoms. Moreover, this spectrum is different from the recorded ^{13}C spectrum of 1,6-diaminohexane, which displays the three expected signals at δ values of 41.8 (assigned to the C atoms attached to nitrogen), 32.8 (assigned to the C atoms at the 2 and 5 positions) and 26.8 (assigned to the C atoms at the 3 and 4 positions). All the above results indicate that our starting material (\pm)-*trans*-1,2-diaminocyclohexane is pure, and not contaminated with 1,6-diaminohexane.

The molar conductivity (Λ_{M}) values of 10^{-3} M solutions of **1–11** are in the range of 85–110 $\text{S cm}^2 \text{mol}^{-1}$ indicating 1 : 3 electrolytes³³ and the decomposition of the complexes in solution.

Description of the structures

The aspects of the molecular and crystal structures of complexes **3**, **5**, **6**, and **8** are shown in Fig. 1, 2 and S5–S9.† The five complexes are isomorphous since (i) the structures all have the same space group and quite similar cell dimensions, and (ii) the types and the positions of atoms in the structures are the same except for a replacement of the Ln^{III} atoms. To facilitate molecular comparison, the same numbering scheme has been assigned to all five complexes presented herein. Thus, only the molecular and crystal structures of compound **1** will be presented in detail.



Scheme 2 Schematic illustration of the *E,E* configuration of LH_2 as observed in its single-crystal X-ray structure.²¹



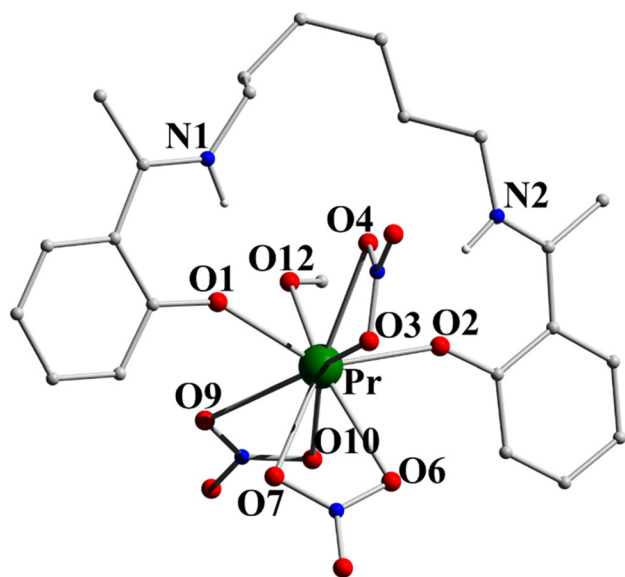


Fig. 1 Partially labelled plot of the structure of the molecule $[\text{Pr}(\text{NO}_3)_3(\text{L}'\text{H}_2)(\text{MeOH})]$ that is present in complex **1**. Most H atoms are omitted for clarity. Selected bond lengths (Å): Pr–O1 2.334(2), Pr–O2 2.337(2), Pr–O12 2.501(2), Pr–O(nitrato) 2.534(2)–2.616(2).

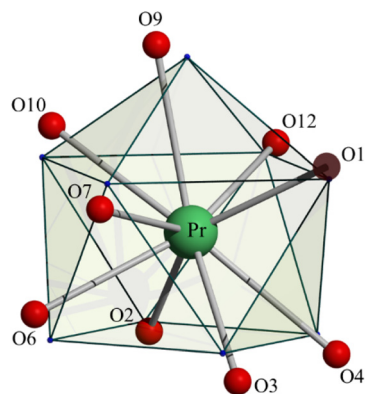


Fig. 2 The spherical capped square antiprismatic coordination polyhedron of Pr^{III} in complex **1**. The very small spheres define the vertices of the ideal polyhedron.

The crystal structure of **1** consists of $[\text{Pr}(\text{NO}_3)_3(\text{L}'\text{H}_2)(\text{MeOH})]$ molecules. The 9-coordinate Pr^{III} centre is bound to six oxygen atoms from the three slightly anisobidentate chelating nitrate groups, two oxygen atoms that belong to the bidentate chelating $\text{L}'\text{H}_2$ ligand and one oxygen atom from the coordinated MeOH molecule. The acidic H atoms, which are bound to the oxygen atoms of the hydroxyl groups in the structure of the free ligand,²¹ are clearly located on the imino nitrogen atoms (N1, N2); thus, the formally neutral ligand participates in its bis(zwitterionic) form leaving the oxygen atoms deprotonated, blocking the N coordination sites and forming an unusual 16-membered chelating ring. The two $\text{N}=\text{C}$ (imino)– $\text{C}(\text{aromatic})$ – $\text{C}(\text{aromatic})$ – O parts of the ligand and the Pr^{III} centre are almost coplanar, with the largest deviation

from their best mean plane being that of O2 (0.137(2) Å); the two aromatic rings are also coplanar and the angle between them is 1.2(2)°. The Pr^{III} –O bond lengths fall in the range of 2.334(2)–2.616(2) Å and are typical of 9-coordinate Pr^{III} complexes. The bond lengths of Pr^{III} to deprotonated phenolato oxygens (2.334(2) and 2.337(2) Å) are shorter than the distances of the nitrate groups (2.534(2)–2.616(2) Å) and methanol (2.501(2) Å). There are two strong intramolecular H bonds in the complex molecule (Table S2†) with the protonated nitrogen atoms being the donors and the negatively charged coordinated oxygen atoms being the acceptors.

There are no Platonic, Archimedean and Catalan polyhedra with nine vertices, and also this number of vertices cannot result in prisms or antiprisms. Thus, the only shapes that may be considered are those listed in Table S3.† With the help of program SHAPE,³⁴ the best fit obtained for the Pr^{III} coordination polyhedron is for the spherical capped square antiprism, with the nitrate atom O9 being the capping atom. Since the coordinated nitrate groups impose small coordination angles ($\sim 50^\circ$), the polyhedron is distorted (Fig. 2).

A variety of intermolecular interactions stabilize the crystal structure of **1**. The two molecules of the unit cell form a centrosymmetric dimer bridged by two relatively strong (Table S2†) $\text{O12} \cdots \text{H12} \cdots \text{O11}$ H bonds (Fig. 3) about the centre of symmetry located at $\frac{1}{2}, \frac{1}{2}, \frac{1}{2}$ of the cell. The molecules are further packed in a 3D network through weak $\text{C} \cdots \text{H} \cdots \text{O}$ interactions.

Each analogous Ln–O bond length in the five isomorphous complexes follows the order $\text{Pr} > \text{Sm} > \text{Gd} > \text{Tb} > \text{Ho}$, which is a consequence of the Ln^{III} contraction.

Compounds **1**, **3**, **5**, **6** and **8** are the first structurally characterized complexes of $\text{L}'\text{H}_2$ or/and its anionic form with any metal. Homometallic Ln^{III} complexes of the salicylaldehyde analogues

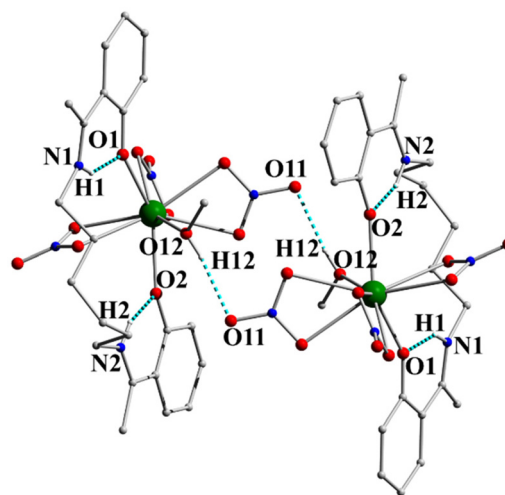


Fig. 3 The centrosymmetric dimeric species $\{[\text{Pr}(\text{NO}_3)_3(\text{L}'\text{H}_2)(\text{MeOH})]\}_2$ formed through intermolecular $\text{O}(\text{methanol})\cdots\text{H}\cdots\text{O}(\text{nitrato})$ H bonds in the crystal structure of **1**. The intramolecular $\text{N}\cdots\text{H}\cdots\text{O}$ H bonds, discussed in the text, are also shown. The Pr^{III} atoms (large spheres) are not labelled for clarity.



of $L'H_2$, i.e. $salhexnH_2$ ³⁵ (Scheme 1), have been reported.³⁶ They are: (i) $\{[Eu_2(hfac)_4(O_2CMe)_2(salhexnH_2)_2]]_n\}$,^{36a} a 1D coordination polymer in which the neutral Schiff-base molecules behave as O, O'-bidentate bridging ligands with the acidic H atoms being located at the oxygen atoms ($hfac^-$ is the hexafluoroacetylacetonato ligand); (ii) $[Eu_2(dbm)_4(O_2CMe)_2(salhexnH_2)_2]$,^{36a} where the two Eu^{III} centres are linked by two O, O'-bidentate bridging ligands with the location of the acidic H atoms being not reported (dbm^- is the dibenzoylmethanide ligand); (iii) $\{[Gd_2(tta)_4(O_2CMe)_2(salhexnH_2)_2]]_n\}$,^{36b} a 1D polymer in which the neutral $salhexnH_2$ molecules behave as O, O'-bidentate bridging ligands with the acidic H atoms being located at the imino nitrogen atoms (tta^- is the 2-thenoyltrifluoroacetylacetonato ligand). Analogous O, O'-bidentate bridging coordination modes have been reported for homometallic Ln^{III} polymers (1D, 2D)^{37,38} and dimers^{36a} possessing the $-(CH_2)_4-$ (i.e. N,N' -bis(salicylidene-1,4-butanediamine)^{36a,37} and $-(CH_2)_5-$ (i.e. N,N' -bis(salicylidene-1,5-pentanediamine)³⁸ analogues of $salhexnH_2$. Thus, the O, O'-bidentate chelating mode of $L'H_2$ in **1–11** is novel in the coordination chemistry of such ligands with aliphatic backbones containing four or more carbon atoms, not only with lanthanoids but also with other metal ions. All the above complexes of the $salhexnH_2$, and $-(CH_2)_4-$ and $-(CH_2)_5-$ analogues were prepared using the open-chain Schiff base which was incorporated in the complexes; no transformation similar to the $LH_2 \rightarrow L'H_2$ one reported in this work was noticed.

Spectroscopic discussion in brief

Representative data are presented in Fig. 4–6 and S10–S12.† The IR spectra of **1–11** are almost identical. The weak-to-medium intensity band at $\sim 3450\text{ cm}^{-1}$ with two submaxima at lower wavenumbers is due to the $\nu(OH)$ vibration of coordinated MeOH³⁹ and the $\nu(NH^+)$ vibration^{15a} of the coordinated $L'H_2$ ligand; the relatively low wavenumber and broadness of the band are both indicative of H bonding, which has been crystallographically confirmed (*vide supra*). The strong band at $\sim 1610\text{ cm}^{-1}$ can be safely assigned to the $\nu(C=N)$ vibration of the protonated imine group. The bands at

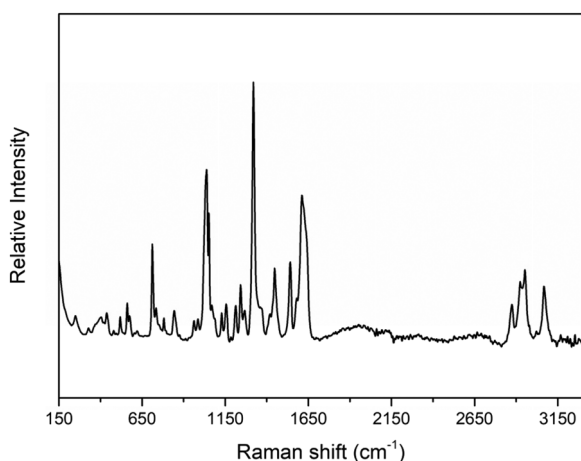


Fig. 4 The Raman spectrum of solid $[Pr(NO_3)_3(L'H_2)(MeOH)]$ (**1**).

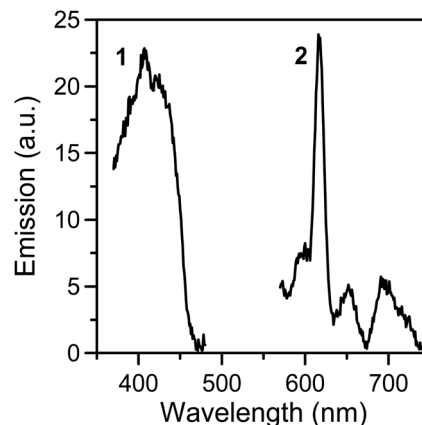


Fig. 5 Solid-state, room-temperature excitation (curve 1; maximum emission at 616 nm) and emission (curve 2; maximum excitation at 399 nm) spectra of solid $[Eu(NO_3)_3(L'H_2)(MeOH)]$ (**4**).

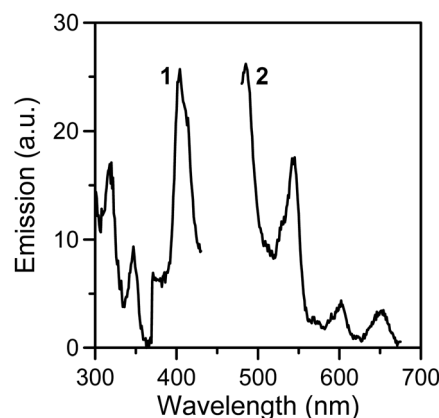


Fig. 6 Solid-state, room-temperature excitation (curve 1; maximum emission at 488 nm) and emission (curve 2; maximum excitation at 405 nm) spectra of solid $[Tb(NO_3)_3(L'H_2)(MeOH)]$ (**6**).

~ 1460 , 1300 cm^{-1} and $\sim 1025\text{ cm}^{-1}$ are assigned⁴⁰ to the vibrational modes $\nu_1(A_1)[\nu(N=O)]$, $\nu_2(B_2)[\nu_{as}(NO_2)]$ and $\nu_2(A_1)[\nu_5(NO_2)]$, respectively, of the bidentate chelating nitrato groups, with the former being possibly overlapped with an aromatic stretch. The separation of the two highest-wavenumber bands is $\sim 160\text{ cm}^{-1}$, which is a typical value of bidentate nitrato ligands. The Raman peaks at 3067, 2953 and 2942, 1611, 1477 and 1267 cm^{-1} (Fig. 4) are due^{40,41} to the $\nu(CH)_{aromatic}$, $\nu(CH)_{aliphatic}$, $\nu(C=N)$, $\nu_1(A_1)[\nu(N=O)]$ and $\nu_5(B_2)[\nu_{as}(NO_2)]$ modes, respectively.

The solid-state, room-temperature luminescence spectra of the Eu^{III} (**4**), Tb^{III} (**6**) and Dy^{III} (**7**) complexes, which are candidates for Ln^{III} -based emission in the visible region,^{12,13} were recorded. Upon maximum excitation at 399 nm, a solid sample of **4** displays photoluminescence with maxima at 595, 616, 652 and 695 nm due to Eu^{III} .^{13a,b,42} These peaks are assigned to the characteristic $^5D_0 \rightarrow ^7F_j$ ($j = 0-4$) transitions. Specific assignments are as follows: $^5D_0 \rightarrow ^7F_{1,2}$ (595 nm), 5D_0

$\rightarrow {}^7\text{F}_2$ (616 nm), ${}^5\text{D}_0 \rightarrow {}^7\text{F}_3$ (652 nm) and ${}^5\text{D}_0 \rightarrow {}^7\text{F}_4$ (695 nm). The dominant peak at 616 nm is due to the hypersensitive ${}^5\text{D}_0 \rightarrow {}^7\text{F}_2$ transition. The higher intensity of this transition compared with that of the magnetic-dipole allowed ${}^5\text{D}_0 \rightarrow {}^7\text{F}_1$ transition indicates that this complex has no imposed symmetry at Eu^{III} , in accordance with our belief that **4** is isomorphous with the structurally characterized complexes **1**, **3**, **5**, **6** and **8**.

Upon maximum excitation at 405 nm, solid **6** displays photoluminescence with maxima at 488, 543, 588, 621 (shoulder) and 648 nm due to Tb^{III} .^{42c,43} These emission maxima are assigned to the transitions from the ${}^5\text{D}_4$ state to its ${}^7\text{F}_6$ (488 nm), ${}^7\text{F}_5$ (543 nm), ${}^7\text{F}_4$ (588 nm), ${}^7\text{F}_3$ (621 nm) and ${}^7\text{F}_2$ (648 nm) states.

The excitation spectrum of complex **7** (Fig. S12†) shows medium-to-strong intensity bands which are attributed⁴⁴ to the appropriate transitions of Dy^{III} : ${}^6\text{H}_{15/2} \rightarrow {}^4\text{M}_{17/2}$, ${}^6\text{P}_{7/2}$ (330 nm), ${}^6\text{H}_{15/2} \rightarrow {}^2\text{K}_{17/2}$ (380 nm) and ${}^6\text{H}_{15/2} \rightarrow {}^4\text{I}_{15/2}$ (418 nm). Upon maximum excitation at 380 nm, solid **7** displays photoluminescence with maxima at 486 and 519 nm being attributed to the intraconfigurational 4f–4f transitions of the metal ion (Fig. S12†).⁴⁴ The maximum located at 486 nm can be safely assigned to the magnetic dipole transition ${}^4\text{F}_{9/2} \rightarrow {}^6\text{H}_{15/2}$, which generally is not sensitive to the crystal field. The expected “yellow” ${}^4\text{F}_{9/2} \rightarrow {}^6\text{H}_{13/2}$ around 575 nm is not observed in our spectrum; this emission is related to the forced electric dipole transition-type and its intensity is strongly influenced (and often strongly quenched) by the crystal-field environment. Thus, the origin of the 519 nm maximum is not clear.

Magnetic studies

Direct current (dc) magnetic susceptibility data on the powdered samples of complexes **5**, **6**, **7** and **8** were collected in the temperature range of 300–2.0 K under an applied field of 0.03 T (Fig. 7 and S13†). The room-temperature $\chi_{\text{M}}T$ values are 7.7 for **5**, 11.9 for **6**, 14.2 for **7** and 13.5 for **8** $\text{cm}^3 \text{K mol}^{-1}$. These values are very close to those expected for the isolated Gd^{III} (${}^8\text{S}_{7/2}$, 7.88 $\text{cm}^3 \text{K mol}^{-1}$), Tb^{III} (${}^7\text{F}_6$, 11.82 $\text{cm}^3 \text{K mol}^{-1}$), Dy^{III}

(${}^6\text{H}_{15/2}$, 14.17 $\text{cm}^3 \text{K mol}^{-1}$) and Ho^{III} (${}^5\text{I}_8$, 14.07 $\text{cm}^3 \text{K mol}^{-1}$) centres, respectively.

Upon cooling, the value of the $\chi_{\text{M}}T$ product for the isotropic (4f^7) Gd^{III} complex **5** is constant down to 25 K and then decreases slowly to a value of 6.0 $\text{cm}^3 \text{K mol}^{-1}$ at 2.0 K. The low-temperature decrease of the product should be attributed to weak intermolecular antiferromagnetic exchange interactions promoted by the two intermolecular $\text{O}_{\text{methanol}}\cdots\text{H}\cdots$ “free” $\text{O}_{\text{nitrate}}\cdots\text{H}$ bonds (*vide supra*, Table S2†) which form $\{\text{Gd}^{\text{III}}\}_2$ dimers. The fit of the experimental data, applying the spin Hamiltonian $H = -2J(\mathbf{S}_1 \cdot \mathbf{S}_2)$, give a satisfactory simulation for $J = -0.03 \text{ cm}^{-1}$ with a g value of 1.98. Magnetization measurements at 2.0 K show a saturation value of $7.03N\mu_{\text{B}}$ in agreement with the expected 7/2 spin. Reduced magnetization data indicate a quasi-negligible anisotropy (Fig. 8, right).

For the Tb^{III} (**6**), Dy^{III} (**7**) and Ho^{III} (**8**) complexes, the values of the $\chi_{\text{M}}T$ product decrease slowly when lowering T due to the progressive depopulation of the m_J levels of the ground state J , with a more pronounced decay below 50 K; the final values at 2.0 K are 7.01 (**6**), 9.21 (**7**) and 5.07 (**8**) $\text{cm}^3 \text{K mol}^{-1}$. The sharp decay at low temperatures might also be due to weak antiferromagnetic $\text{Ln}^{\text{III}}\cdots\text{Ln}^{\text{III}}$ interactions within the H-bonded dimers. The susceptibility data were fitted assuming implicitly a regular distribution of the m_J states. The Hamiltonian used is represented by eqn (1), where \hat{S} is the spin operator, L is the orbit operator,^{45,46} λ is the spin–orbit coupling and Δ describes the energy gap between m_L components. The value for the orbital reduction parameter k was assumed as 1 (the Ln^{III} ions behave as purely ionic). Thus, the first term of the Hamiltonian describes the spin–orbit coupling, the second is related to the ligand field around the lanthanoid cation, and the third term describes the Zeeman effect.

$$H = (\lambda \hat{S}L) + \Delta[L_z^2 - L(L+1)/3] + [\beta H(-k_L + 2\hat{S})] \quad (1)$$

In spite of the low symmetry of the Ln^{III} environment in **6**–**8**, the $\chi_{\text{M}}T$ simulations were accurate with Δ parameters of -37 , -10 and -14 cm^{-1} for **6**, **7** and **8**, respectively. The nega-

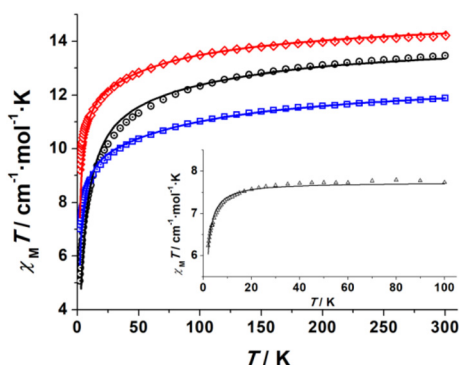


Fig. 7 Temperature dependence of the $\chi_{\text{M}}T$ product at 0.03 T for compounds **6** (squares), **7** (diamonds) and **8** (circles) (main curves). The $\chi_{\text{M}}T$ vs. T (100–2.0 K) variation for complex **5** is shown in the inset. Solid lines show the best fit of the experimental data.

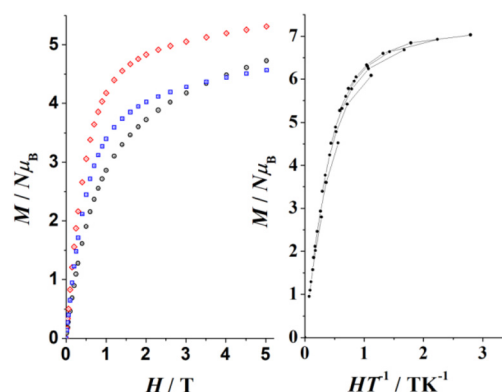


Fig. 8 (Left) Magnetization plots for complexes **6**–**8**; squares, diamonds and circles represent the data for compounds **6**, **7** and **8**, respectively. (Right) Reduced magnetization for Gd^{III} complex **5** between 1.8 and 6.8 K with increments of 1 K.



tive values of Δ indicate that the highest m_j value corresponds to the ground state. The magnetization plots of 6–8 at 2.0 K show a fast increase at a low field with quasi saturation (Fig. 8), confirming the negative Δ values for these complexes.

Ac magnetic susceptibility measurements were performed using a 4.0 G ac field on the powdered samples of 6–8 under different static fields in order to explore the magnetization dynamics of the three complexes. No out-of-phase (imaginary) components of the ac susceptibility, χ''_M , were detected in the Tb^{III} and Ho^{III} complexes at frequencies between 10 and 1488 Hz, either at zero field or under external applied fields. In contrast, Dy^{III} complex 7 exhibits tails of peaks below 5 K as expected for a Kramers' ion with $m_j = \pm 15/2$ ground doublet (Fig. 9, left and S15†). The χ''_M response was measured at zero dc field, and also under applied external (bias) dc fields of 0.1 and 0.2 T without observing any enhancement of the peaks' maxima; this indicates that the quantum tunnelling of the magnetization (QTM) is not the relaxation path in this case despite the distorted environment around the Dy^{III} centre. Due to the lack of maxima in the 10–1480 Hz frequency range and in the measured temperature range, the system was fitted (Fig. 9, right and S14†) according to the Debye eqn (2),⁴⁷ giving the mean values of 4.6 cm⁻¹ and 7.6×10^{-7} s for the effective barrier for the magnetization reversal (U_{eff}) and pre-experimental factor (τ_0), respectively. The experimental data were not enough for a complete Cole–Cole plot to investigate the magnetic relaxation mechanism; however, due to the U_{eff} value which is smaller than the energy of the first excited state, the Orbach relaxation is discarded as the main relaxation path.

$$\ln(\chi''_M/\chi'_M) = \ln(\omega\tau_0) - U_{\text{eff}}/k_B T \quad (2)$$

Given the recent discovery of and great interest on Gd^{III} SIMs/SMs,^{48,49} we investigated the dynamic properties of 5. Out-of-phase magnetic susceptibility signals were not observed at zero field, but upon increasing the static (dc) field tails of signals appeared with a maximum intensity around 0.4 T. The χ''_M versus T measurements were carried out at this field in the

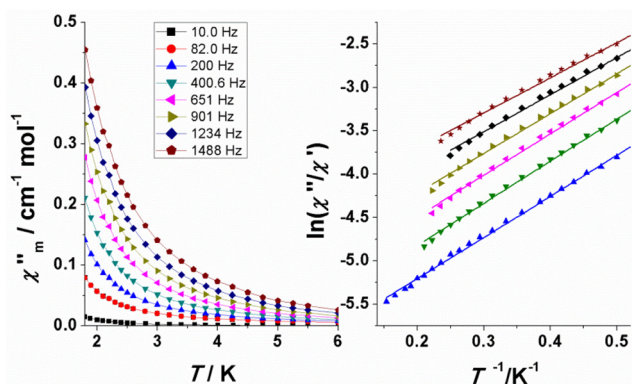


Fig. 9 Ac data for complex 7. (Left) Out-of-phase magnetic susceptibility (χ''_M) versus T in a 4.0 G ac field oscillating between 1488 and 10 Hz at zero static (dc) field. (Right) Natural logarithm of χ''_M/χ'_M versus $1/T$ at different ac frequencies (1488–200 Hz) in zero static (dc) field.

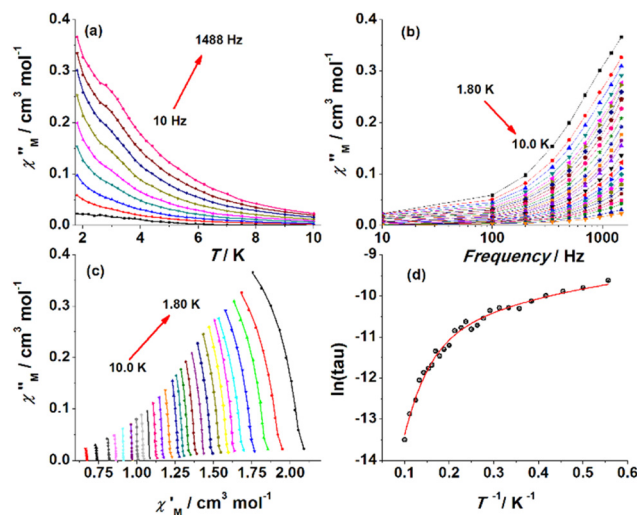


Fig. 10 Top, temperature dependence (a) and frequency dependence (b) of χ''_M for complex 5 under a 0.4 T static field. Bottom, Argand plot (c) and fit of the $\ln(\tau)$ vs. inverse of temperature (d).

10–1488 Hz range and a clear frequency dependence was observed, Fig. 10. The $\chi''_M(T)$ plot shows two processes, one as a shoulder signal at higher frequencies around 2.5 K and a second one below 1.8 K, which are almost completely overlapped showing that the two different magnetic relaxation paths are occurring at very close temperatures (Fig. 10, top). A fit of the Argand plot performed by the generalized Debye model shows an α parameter with values between 0.06 and 0.16 indicating a narrow distribution of relaxation times and short τ values in the 10^{-5} – 10^{-6} s interval which are shown as $\ln(\tau)$ vs. the inverse of temperature in Fig. 10, bottom and S14.† Fitting of the $\ln(\tau)$ plot can be performed with similar quality factors combining several relaxation mechanisms such as Orbach plus Raman, Orbach plus direct or direct plus Raman. However, taking into account that the conventional U_{eff} barrier derived from a double-well potential cannot be applied for this kind of quasi-isotropic system ($DS^2 \ll kT$), the only realistic fit is from the direct (low temperature) plus Raman (high temperature, *via* lattice vibrations) relaxation combination applying the expression:

$$\tau^{-1} = AT + CT^n \quad (3)$$

The best fit values were $A = 9136$, $C = 6.85$ and $n = 4.90$, Fig. 10 bottom. The n value is lower than the theoretical $n = 9$ value for the Kramers ions but is commonly attributed to the participation of optical lattice vibrations, which has been previously reported.⁵⁰

Complex 5 joins a limited number of Gd^{III} complexes exhibiting slow relaxation of the magnetization in spite of the isotropic character of the cation, which contrasts with the classical interpretation for the slow relaxation of the magnetization usually explained as an over barrier process depending on the axial zero field splitting. The mostly accepted explanation^{48a,g,h,49} is the presence of a weak axial zero-field



splitting ($D \sim 0.1 \text{ cm}^{-1}$), which cannot be detected by magnetization or susceptibility studies. These small values, which result from molecular distortion, allow very small double-well energy barriers around $\sim 1 \text{ cm}^{-1}$ (calculated by the formula $DS^2 - 1/4$), which are in the orders of magnitude lower than the experimentally calculated barriers (U_{eff}). Such low D values, however, imply that the relaxation phenomenon cannot be explained in terms of conventional over-barriers or QTM above 2 K. The weak anisotropy breaks the degeneration at the $S = 7/2$ level, mixing the m_s sublevels under moderate ($\sim 0.4 \text{ T}$) external magnetic fields and resulting in SIM/SMM behaviour.

Concluding comments and perspectives

It is rather difficult to conclude on a research project which is still at its infancy. The most salient features of this work are: (1) the first use of the tetradentate Schiff base LH_2 (Schemes 1 and 2) has provided access to an interesting family of mononuclear Ln^{III} complexes. (2) The original ligand LH_2 has undergone a novel Ln^{III} -assisted $\text{LH}_2 \rightarrow \text{L}'\text{H}_2$ transformation and the resulting complexes contain the latter as the ligand; a mechanistic scheme for this transformation has been proposed (ESI†). These preliminary results may give “food for thought” concerning the potential use of Ln^{III} ions as catalysts in ring-opening reactions of cyclohexane-containing substrates in MeOH under mild conditions. (3) The $\text{L}'\text{H}_2$ ligand is incorporated in its bis (zwitterionic) form and exhibits a new coordination mode (O, O' -chelating) for this type of Schiff base. (4) The Eu^{III} , Tb^{III} and Dy^{III} complexes display Ln^{III} -based emission in the visible region proving that the coordinated $\text{L}'\text{H}_2$ molecule can effectively transfer energy to the excited, emissive levels of these Ln^{III} ions; (5) The Dy^{III} member of the family is a weak SMM at zero external field, and the QTM or Orbach processes are not the relaxation paths; the Gd^{III} compound exhibits SIM properties under a moderate external dc field, thus joining a small group of such complexes.

Our future directions in the project include: (a) Reactions of LH_2 with 3d and 5f (uranyl, thorium(IV)) ions to see if the $\text{LH}_2 \rightarrow \text{L}'\text{H}_2$ transformation can be observed again; preliminary experiments indicate that 3d-metal complexes containing either LH_2 or $\text{L}'\text{H}_2$ can be isolated. For example, compounds $\{\text{Fe}^{\text{III}}\text{Cl}_3(\text{LH}_2) \cdot \text{Et}_2\text{O}\}_n$, $\{[\text{Fe}^{\text{III}}\text{Cl}_3(\text{LH}_2) \cdot 2\text{Me}_2\text{CO}]_n$ and $\{[\text{Mn}^{\text{II}}\text{Cl}_2(\text{LH}_2)_2] \cdot 3\text{MeOH}\}_n$ have been recently structurally characterized, depending on the reaction conditions. Complex $(\text{Et}_3\text{NH})[\text{Mn}^{\text{III}}(\text{L})_2(\text{L}'\text{H}_2)](\text{ClO}_4)_3 \cdot \text{CHCl}_3$, which contains both the original and transformed ligands, can be isolated from the 1 : 1 : 2 $\text{Mn}(\text{ClO}_4)_2 \cdot 6\text{H}_2\text{O}/\text{LH}_2/\text{Et}_3\text{N}$ reaction mixture in CHCl_3 -MeOH (Fig. S16–S19†) (b) Synthesis and full characterization of $\text{L}'\text{H}_2$ (this compound is not known), followed by its reaction with lanthanoid(III) nitrates to investigate if the same complexes (1–11) with those described here can be obtained. (c) Reactions of ligands analogous to LH_2 , but possessing various substituents ($-\text{Cl}$, $-\text{Br}$, $-\text{Me}$, ...) on the aromatic rings, with Ln^{III} ions to investigate if the identity of the products depends

on the nature of the substituent and if similar metal ion-assisted transformations are operative; (d) reactions of Schiff bases derived from the 2 : 1 condensation between 2-hydroxyacetophenone and 1,2-diaminocyclopentane or 1,2-diaminocyclobutane with Ln^{III} ions; the ring-opening process might be easier with such Schiff bases given the larger strain of these rings than that in cyclohexane (cyclobutane 27 kcal mol^{-1} , cyclopentane 5 kcal mol^{-1} , and cyclohexane 1 kcal mol^{-1}).

Author contributions

I. M.-M.: conceptualization, synthesis, and data analysis; Z. L.: Raman spectroscopy and data analysis; A. K.: synthesis and conventional characterization; D. M.: synthesis and conventional characterization; K. Skordi: collection of single-crystal crystallographic data; A. T.: supervision of the experimental work on single-crystal crystallography; V. B.: luminescence spectra and data analysis; A. E.: supervision of the experimental magnetic work; J. M. magnetic measurements, data analysis, and writing of the magnetic part of the manuscript; V. N.: solution and refinement of the single-crystal X-ray structures and creation of structural plots; E. B.: theoretical calculations and writing of the relevant part of the manuscript; D. P.: mechanistic proposals and writing of the relevant part of the manuscript; S. P.: conceptualization, supervision, project management, and final manuscript writing and editing.

Conflicts of interest

There are no conflicts of interest to declare.

Acknowledgements

We thank Research Director George Voyiatzis for permitting us to use the Raman facilities at ICE-HT/FORTH. AE and JM are grateful for the funding from MICINN (Project PGC2018-094031-B-I00). We also thank the undergraduate student Chrysanthi Panteli for preliminary synthetic work and the PhD candidate Eleanna Vahlioti for her assistance to obtain the NMR spectra.

References

- 1 J. Ribas Gispert, *Coordination Chemistry*, Wiley-VCH, Weinheim, Germany, 2008, pp. XXIV–XXXVII.
- 2 J.-P. Launay and M. Verdaguer, *Electrons in Molecules*, Oxford University Press, Oxford, UK, revised edition, 2018.
- 3 J. C. Wedal and W. J. Evans, *J. Am. Chem. Soc.*, 2021, **143**, 18354–18367 (perspective).
- 4 For an excellent essay, see: T. Cheisson and E. J. Schelter, *Science*, 2019, **363**, 489–493.
- 5 N. Ishikawa, M. Sugita, T. Ishikawa, S.-Y. Koshihara and Y. Kaizu, *J. Am. Chem. Soc.*, 2003, **125**, 8694–8695.



- 6 J. Tang and P. Zhang, *Lanthanide Single Molecule Magnets*, Springer-Verlag, Berlin, Germany, 2015.
- 7 For representative review-type articles, see: (a) N. F. Chilton, *Ann. Rev.*, 2022, **52**, 79–101; (b) D. N. Woodruff, R. E. P. Winpenney and R. A. Layfield, *Chem. Rev.*, 2013, **113**, 5110–5148; (c) A. Zabala-Lekuona, J. M. Seco and E. Colacio, *Coord. Chem. Rev.*, 2021, **441**, 213984; (d) P. Zhang, L. Zhang and J. Tang, *Dalton Trans.*, 2015, **44**, 3923–3929 (frontier); (e) S. T. Liddle and J. van Slageren, *Chem. Soc. Rev.*, 2015, **44**, 6655–6669; (f) F. Pointillart, O. Cadoret, B. Le Guennic and L. Ouahab, *Coord. Chem. Rev.*, 2017, **346**, 150–175; (g) J.-L. Liu, Y.-C. Chen and M.-L. Tong, *Chem. Soc. Rev.*, 2018, **47**, 2431–2453; (h) S. K. Gupta and R. Murugavel, *Chem. Commun.*, 2018, **54**, 3685–3696 (feature article); (i) K. L. M. Harriman, D. Errulat and M. Murugesu, *Trends Chem.*, 2019, **1**, 425–439; (j) R. Sessoli and A. K. Powell, *Coord. Chem. Rev.*, 2009, **253**, 2328–2341; (k) F. Habib and M. Murugesu, *Chem. Soc. Rev.*, 2013, **42**, 3278–3288; (l) K. Katoh, T. Komeda and M. Yamashita, *Chem. Rec.*, 2016, **16**, 987–1016.
- 8 J. D. Rinehart and J. R. Long, *Chem. Sci.*, 2011, **2**, 2078–2085 (perspective).
- 9 (a) T. Fukuda, N. Shigeyoshi, T. Yamamura and N. Ishikawa, *Inorg. Chem.*, 2014, **53**, 9080–9086; (b) A. Lunghi, F. Totti, R. Sessoli and S. Sanvito, *Nat. Commun.*, 2017, **8**, 14620.
- 10 (a) F.-S. Guo, B. M. Day, Y.-C. Chen, M.-L. Tong, A. Mansikkamäki and R. A. Layfield, *Angew. Chem., Int. Ed.*, 2017, **56**, 11445–11449; (b) C. A. P. Goodwin, F. Ortu, D. Reta, N. F. Chilton and D. P. Mills, *Nature*, 2017, **548**, 439–442.
- 11 (a) K. R. McClain, C. A. Gould, K. Chakarawet, S. J. Teat, T. J. Groshens, J. R. Long and B. G. Harvey, *Chem. Sci.*, 2018, **9**, 8492–8503; (b) C. A. Gould, K. R. McClain, J. M. Yu, T. J. Groshens, F. Furche, B. G. Harvey and J. R. Long, *J. Am. Chem. Soc.*, 2019, **141**, 12967–12973; (c) F.-S. Guo, D. M. Day, Y.-C. Chen, M.-L. Tong, A. Mansikkamäki and R. A. Layfield, *Science*, 2018, **362**, 1400–1403.
- 12 H. C. Aspinall, *f-Block Chemistry*, Oxford University Press, Oxford, UK, 2020, pp. 13–14, 28–32.
- 13 (a) J.-C. G. Bünzli, *Coord. Chem. Rev.*, 2015, **293–294**, 19–47; (b) L. Armelao, S. Quici, F. Barigelli, G. Accorsi, G. Bottaro, M. Cavazzini and E. Tondello, *Coord. Chem. Rev.*, 2010, **254**, 487–505; (c) J. Andres and K. E. Borbas, *Inorg. Chem.*, 2015, **54**, 8174–8176; (d) J. Vuojola and T. Soukka, *Methods Appl. Fluoresc.*, 2014, **2**, 1–27.
- 14 For example, see: (a) J. Long, I. V. Basalov, N. V. Forosenko, K. A. Lyssenko, E. Mamantova, A. V. Cherkasov, M. Damjanović, L. F. Chibotaru, Y. Guari, J. Larionova and A. A. Trifonov, *Chem. – Eur. J.*, 2019, **25**, 474–478; (b) K. Kobayashi, Y. Harada, K. Ikenaga, Y. Kitagawa, M. Nakano and T. Kajiura, *Magnetochemistry*, 2019, **5**, 27; (c) Y. Yao, H.-Y. Yin, Y. Ning, J. Wang, Y.-S. Meng, X. Huang, W. Zhang, L. Kang and J.-L. Zhang, *Inorg. Chem.*, 2019, **58**, 1806–1814.
- 15 For example see: (a) D. Maniaki, I. Mylonas-Margaritis, J. Mayans, A. Savvidou, C. P. Raptopoulou, V. Bekiari, V. Psycharis, A. Escuer and S. P. Perlepes, *Dalton Trans.*, 2018, **47**, 11859–11872; (b) I. Mylonas-Margaritis, D. Maniaki, J. Mayans, L. Ciammaruchi, V. Bekiari, C. P. Raptopoulou, V. Psycharis, S. Christodoulou, A. Escuer and S. P. Perlepes, *Magnetochemistry*, 2018, **4**, 45.
- 16 C. Camp, V. Guidal, B. Biswas, J. Pécaut, L. Dubois and M. Mazzanti, *Chem. Sci.*, 2012, **3**, 2433–2448.
- 17 K. S. Pedersen, A.-M. Ariciu, S. McAdams, H. Weihe, J. Bendix, F. Tuna and S. Piligkos, *J. Am. Chem. Soc.*, 2016, **138**, 5801–5804.
- 18 R. Hussain, G. Allodi, A. Chiesa, E. Garlatti, D. Mitcov, A. Konstantatos, K. S. Pedersen, R. De Renzi, S. Piligkos and S. Carretta, *J. Am. Chem. Soc.*, 2018, **140**, 9814–9818.
- 19 J. Cheng, Y. Li, R. Sun, J. Liu, F. Gou, X. Zhou, H. Xiang and J. Liu, *J. Mater. Chem. C*, 2015, **3**, 11099–11110.
- 20 (a) G.-L. Wang, Y.-M. Tian, D.-X. Cao, Y.-S. Yu and W.-B. Sun, *Z. Anorg. Allg. Chem.*, 2011, **637**, 583–588; (b) G.-L. Wang, Y.-M. Tian, W.-B. Sun, B.-L. Han, M.-F. Yu, H. Xu and T. Gao, *Z. Anorg. Allg. Chem.*, 2011, **637**, 1616–1621; (c) J. Zhu, H.-F. Song, P.-F. Yan, G.-F. Hou and G.-M. Li, *Cryst. Eng. Commun.*, 2013, **15**, 1747–1752; (d) Q. Liu, M. Ding, Y. Lin and Y. Xing, *Polyhedron*, 1998, **17**, 555–559; (e) Q. Liu and M. Ding, *J. Organomet. Chem.*, 1998, **553**, 179–181; (f) Q. Liu, J. Huang, Y. Qian and A. S. C. Chan, *Polyhedron*, 1999, **18**, 2345–2350; (g) J. Zhu, H. Song, J. Sun, P. Yan, G. Hou and G. Li, *Synth. Met.*, 2014, **192**, 29–36; (h) P.-F. Yan, P.-H. Lin, F. Habib, T. Aharen, M. Murugesu, Z.-P. Deng, G.-M. Li and W.-B. Sun, *Inorg. Chem.*, 2011, **50**, 7059–7065; (i) J.-W. Sun, J. Zhu, H.-F. Song, G.-M. Li, X. Yao and P.-F. Yan, *Cryst. Growth Des.*, 2014, **14**, 5356–5360; (j) X. Zou, C. Du, Y. Dong and G. Li, *Inorg. Chim. Acta*, 2020, **507**, 119455.
- 21 F. Chen and H.-Y. Ye, *Acta Crystallogr., Sect. E: Struct. Rep. Online*, 2008, **64**, o1757.
- 22 *Crysalis PRO (version 1.171.93)*, Rigaku Oxford Diffraction, Yarnton Oxfordshire, UK, 2018.
- 23 (a) G. M. Sheldrick, *Acta Crystallogr., Sect. A: Found. Adv.*, 2015, **71**, 3–8; (b) G. M. Sheldrick, *Acta Crystallogr., Sect. C: Struct. Chem.*, 2015, **71**, 3–8.
- 24 A. Spek, *Acta Crystallogr., Sect. D: Struct. Biol.*, 2009, **65**, 148–155.
- 25 O. V. Dolomanov, L. J. Bourhis, R. J. Gildea, J. A. K. Howard and H. Puschmann, *J. Appl. Crystallogr.*, 2009, **42**, 339–341.
- 26 L. Farrugia, *J. Appl. Crystallogr.*, 2012, **45**, 849–854.
- 27 K. Branderburg, *DIAMOND: Program for Crystal and Molecular Structure Visualization*, Crystal Impact Gbr, Bonn, Germany, 2014.
- 28 C. F. Macrae, I. Sovago, S. J. Cottrell, P. T. A. Galek, P. McCabe, E. Pidcock, M. Platings, G. P. Shields, J. S. Stevens, M. Towler and P. A. Wood, *J. Appl. Crystallogr.*, 2020, **53**, 226–235.
- 29 M. J. Frisch, G. W. Trucks, H. B. Schlegel, G. E. Scuseria, M. A. Robb, J. R. Cheeseman, G. Scalmani, V. Barone, B. Mennucci, G. A. Petersson, H. Nakatsuji, M. Caricato,



- X. Li, H. P. Hratchian, A. F. Izmaylov, J. Bloino, G. Zheng, J. L. Sonnenberg, M. Hada, M. Ehara, K. Toyota, R. Fukuda, J. Hasegawa, M. Ishida, T. Nakajima, Y. Honda, O. Kitao, H. Nakai, T. Vreven, J. A. Montgomery Jr., J. E. Peralta, F. Ogliaro, M. Bearpark, J. J. Heyd, E. Brothers, K. N. Kudin, V. N. Staroverov, T. Keith, R. Kobayashi, J. Normand, K. Raghavachari, A. Rendell, J. C. Burant, S. S. Iyengar, J. Tomasi, M. Cossi, N. Rega, J. M. Millam, M. Klene, J. E. Knox, J. B. Cross, V. Bakken, C. Adamo, J. Jaramillo, R. Gomperts, R. E. Stratmann, O. Yazyev, A. J. Austin, R. Cammi, C. Pomelli, J. W. Ochterski, R. L. Martin, K. Morokuma, V. G. Zakrzewski, G. A. Voth, P. Salvador, J. J. Dannenberg, S. Dapprich, A. D. Daniels, O. Farkas, J. B. Foresman, J. V. Ortiz, J. Cioslowski and D. J. Fox, *Gaussian 09, Revision B.01*, Gaussian, Inc., Wallingford CT, 2010.
- 30 M. Dolg, H. Stoll and H. Preuss, *Theor. Chim. Acta*, 1993, **85**, 441–450.
- 31 For example, see: (a) G. A. Molander, *Chem. Rev.*, 1992, **92**, 29–68; (b) W. S. Trahanovsky, L. H. Young and M. H. Bierman, *J. Org. Chem.*, 1969, **34**, 869–871.
- 32 E. Szlyk, A. Wojtczak, E. Larsen, A. Surdykowski and J. Neumann, *Inorg. Chim. Acta*, 1999, **293**, 239–244.
- 33 W. J. Geary, *Coord. Chem. Rev.*, 1971, **7**, 81–122.
- 34 M. Llunell, D. Casanova, J. Girera, P. Alemany and S. Alvarez, *SHAPE, version 2.0*, Barcelona, Spain, 2010.
- 35 I. Sheikshoae and M. A. Sharif, *Acta Crystallogr., Sect. E: Struct. Rep. Online*, 2006, **62**, o3563–o3565.
- 36 (a) T. Koizuka, K. Yanagisawa, Y. Hirai, Y. Kitagawa, T. Nakanishi, K. Fushimi and Y. Hasegawa, *Inorg. Chem.*, 2018, **57**, 7097–7103; (b) Y.-Y. Xu, O. Sun, Y. Qi, B.-Y. Xie and T. Gao, *New J. Chem.*, 2019, **43**, 16706–16713; (c) Y.-Y. Xu, P. Chen, T. Gao, H.-F. Li and P.-F. Yan, *Cryst. Eng. Commun.*, 2019, **21**, 5965–5972.
- 37 (a) Y. Yue, G. Hou, X. Yao and G. Li, *Polyhedron*, 2017, **129**, 157–163; (b) Y. Yue, P. Yan, J. Sun, G. Hou and G. Li, *Polyhedron*, 2015, **94**, 90–95; (c) Y. Jia, H. Li, P. Chen, T. Gao, W. Sun and P. Yan, *Aust. J. Chem.*, 2018, **71**, 527–533; (d) W. Radecka-Paryzek, I. Pospieszna-Markiewicz and M. Kubicki, *Inorg. Chim. Acta*, 2007, **360**, 488–496; (e) Y. Yue, P. Yan, J. Sun and G. Li, *Inorg. Chem. Commun.*, 2015, **54**, 5–8; (f) Y. Yue, J. Sun, P. Yan and G. Li, *Inorg. Chem. Commun.*, 2015, **51**, 42–45; (g) I. Pospieszna-Markiewicz, M. T. Kaczmarek, M. Kubicki and W. Radecka-Paryzek, *J. Alloys Compd.*, 2008, **451**, 403–405.
- 38 W. Radecka-Paryzek, I. Pospieszna-Markiewicz and M. Kubicki, *J. Rare Earths*, 2010, **28**, 51–55.
- 39 C. Stamou, Z. G. Lada, C. T. Chasapis, D. Papaioannou, P. Dechambenoit and S. P. Perlepes, *Dalton Trans.*, 2022, **51**, 15771–15782.
- 40 K. Nakamoto, *Infrared and Raman Spectra of Inorganic and Coordination Compounds*, Wiley, New York, USA, 4th edn, 1986, pp. 254–257.
- 41 F. R. Dollish, W. G. Fateley and F. F. Bentley, *Characteristic Raman Frequencies of Organic Compounds*, Wiley, New York, USA, 1974, pp. 1–4, 136, 175–179.
- 42 (a) C. D. Polyzoou, H. Nikolaou, C. P. Raptopoulou, K. F. Konidaris, V. Bekiari, V. Psycharis and S. P. Perlepes, *Molecules*, 2021, **26**, 1622; (b) H. Nikolaou, A. Terzis, C. P. Raptopoulou, V. Psycharis, V. Bekiari and S. P. Perlepes, *J. Surf. Interf. Mater.*, 2014, **2**, 311–318; (c) V. Bekiari, K. A. Thiakou, C. P. Raptopoulou, S. P. Perlepes and P. Lianos, *J. Lumin.*, 2008, **128**, 481–488.
- 43 S. Kalusniak, E. Castellano-Hernández, H. Yalçinoğlu, H. Tanaka and C. Kränkel, *Appl. Phys. B*, 2022, **128**, 33.
- 44 S. Chemingui, M. Ferhi, K. Horchani-Naifer and M. Férid, *J. Lumin.*, 2015, **166**, 82–87.
- 45 M. V. Marinho, D. O. Reis, W. X. C. Oliveira, L. F. Marques, H. O. Stumpf, M. del Déniz, J. Pasán, C. Ruiz-Pérez, J. Cano, F. Lloret and M. Julve, *Inorg. Chem.*, 2017, **56**, 2108–2123.
- 46 E. Pilichos, À. Tubau, S. Speed, M. Font-Bardia, A. Escuer, A. Grabulosa and J. Mayans, *Dalton Trans.*, 2023, **52**, 2485–2494.
- 47 J. Bartolomé, G. Filoti, V. Kuncser, G. Schienteie, V. Mereacre, C. E. Anson, A. K. Powell, D. Prodius and C. Turta, *Phys. Rev. B: Condens. Matter Mater. Phys.*, 2009, **80**, 014430.
- 48 For example, see: (a) M. Orendáč, L. Sedláková, E. Čizmar, A. Orendáčová, A. Feher, S. A. Zvyagin, J. Wosnitza, W. H. Zhu, Z. M. Wang and S. Gao, *Phys. Rev. B: Condens. Matter Mater. Phys.*, 2010, **81**, 214410; (b) A. Arauzo, A. Lazarescu, S. Shova, E. Bartolomé, R. Cases, J. Luzón, J. Bartolomé and C. Turta, *Dalton Trans.*, 2014, **43**, 12342–12356; (c) M. J. Martínez-Pérez, S. Carbona-Serra, C. Schlegel, F. Moro, P. J. Alonso, H. Prima-García, J. M. Clemente-Juan, M. Evangelisti, A. Gaita-Ariño, J. Sesé, J. van Slageren, E. Coronado and F. Luis, *Phys. Rev. Lett.*, 2012, **108**, 247213; (d) A. Vráblová, M. Tomás, L. R. Falvello, L. Dlhán, J. Titiš, J. Černák and R. Boča, *Dalton Trans.*, 2019, **48**, 13943–13952; (e) T. K. Ghosh, S. Maity, J. Mayans and A. Ghosh, *Inorg. Chem.*, 2021, **60**, 438–448; (f) M. Orts-Arroyo, R. Rabelo, A. Carrasco-Berlanga, N. Moliner, J. Cano, M. Julve, F. Lloret, G. De Munno, R. Ruiz-García, J. Mayans, J. Martínez-Lillo and I. Castro, *Dalton Trans.*, 2021, **50**, 3801–3805; (g) Y. Horii, K. Katoh, Y. Miyazaki, M. Damjanovic, T. Sato, L. Ungur, L. F. Chibotaru, B. K. Breedlove, M. Nakano, W. Wernsdorfer and M. Yamashita, *Chem. – Eur. J.*, 2020, **26**, 8076–8082; (h) E. Pilichos, M. Font-Bardia, A. Escuer and J. Mayans, *Dalton Trans.*, 2021, **50**, 1746–1753; (i) R. J. Holmberg, L. T. A. Ho, L. Ungur, I. Korobkov, L. F. Chibotaru and M. Murugesu, *Dalton Trans.*, 2015, **44**, 20321–20325.
- 49 J. Mayans and A. Escuer, *Chem. Commun.*, 2021, **57**, 721–724.
- 50 L. Gu and R. Wu, *Phys. Rev. B: Condens. Matter Mater. Phys.*, 2021, **103**, 014401.

